Wang and Choi
Micro and Nano Systems Letters (2023) 11:5
https://doi.org/10.1186/s40486-023-00171-0

Micro and Nano Systems Letters

LETTER

Open Access

Improved recovery of NO_2 sensors using heterojunctions between transition metal dichalcogenides and ZnO nanoparticles

Leilei Wang[1] and Jungwook Choi[1*]

Abstract

The stable recovery of gas sensors is an important indicator for evaluating their performance. Hitherto, the use of external light sources and/or an increase in the operating temperature has been effective in improving the recovery rate of gas sensors. Herein, heterojunctions were formed between the two-dimensional transition metal dichalcogenide nanosheets and zero-dimensional ZnO nanoparticles to improve the recovery rate of a NO_2 sensor. Scanning electron microscopy and Raman spectroscopy suggested a successful deposition of ZnO nanoparticles onto the MoS_2 and WSe_2 nanosheets. The sensing response to 10 ppm NO_2 gas at 100 °C indicated that the heterojunction formed by ZnO and MoS_2 or WSe_2 successfully improved the recovery rate of the sensor by 11.87% and 19.44%, respectively, whereas the sensitivity remained constant. The proposed approach contributes to improving the performance of gas sensors.

Keywords Heterojunction, Molybdenum disulfide, Tungsten diselenide, Gas sensing, Recovery

Introduction

Nitrogen dioxide (NO_2) is considered a major pollutant affecting the environment and human health [1, 2]. In the past few decades, nanomaterials, such as metal oxides [3–5], transition metal dichalcogenides (TMDC) [6–8], and carbon-based materials [9–12], have been used as sensing layers of the chemiresistors to detect NO_2 gas. An ideal gas sensor should exhibit high sensitivity, fast response, full recovery, and a low detection limit.

Carbon-based materials, such as graphene and carbon nanotubes (CNT), have been widely studied owing to their excellent electrical conductivity, stability, high surface-to-volume ratios, and low toxicity [13–15]. Carbon-based NO_2 gas sensors exhibit excellent responses to ppb-level NO_2 at room temperature. However, these sensors often require prolonged recovery times because of the strong bonding between NO_2 molecules and the sp^2-carbon in carbon-based materials [16, 17], which significantly affects the overall performance of the carbon-based gas sensors.

On the other hand, metal oxide-based NO_2 gas sensors, such as ZnO, TiO_2, WO_3, In_2O_3, and SnO_2, offer several advantages, including rapid response, high sensitivity, simplicity, and easy synthesis [18–23]. In particular, ZnO has garnered significant attention owing to its stable chemical and physical properties, simple synthesis, cost-effectiveness, and nontoxicity. ZnO has been widely employed in the fabrication of gas sensors in various forms, including nanowires [24], nanorods [25], and nanoflakes [26]. However, the ZnO-based gas sensors typically require operating temperatures higher than 200 °C [16, 27–29].

Gas sensors based on TMDC, such as MoS_2, WS_2, and WSe_2, can detect NO_2 and NH_3 gases at room temperature [30–34] owing to their distinctive layered structures, unique photoelectric and charge transfer properties, air

*Correspondence:
Jungwook Choi
choij@cau.ac.kr
[1] School of Mechanical Engineering, Chung-Ang University, Seoul 06974, Republic of Korea

stability, and presence of abundant active sites (e.g., sulfur vacancies and edge sites) [35–38]. However, low sensitivity, slow response, and poor recovery are the major limitations associated with TMDC-based NO_2 gas sensors [39–41].

Chemical doping [42], exposed edge positions [43], photoactivation [44], and noble metal/other nanomaterial functionalization [45–47] have been employed to enhance the sensitivity of sensors. Furthermore, recovery rate, which is one of the critical performance indicators for sensors, needs to be improved. Heterojunctions, external light assistance, and high operating temperatures have been reported to improve sensor recovery rate [15, 44, 48–50]. Among them, heterojunctions have received significant attention because of their energy-saving capabilities.

In this study, heterojunctions were fabricated to improve the recovery of TMDC-based gas sensors. The recovery rate of the sensors could be improved by approximately 5.72–11.87% and 8.10–19.44% via spray-coating of a small amount of n-type ZnO nanoparticles onto the p-type MoS_2 and WSe_2 nanosheets, respectively.

Results and discussion

The TMDC and diluted ZnO dispersions are successively spray-coated onto a SiO_2 wafer with an interdigitated Au electrode to form a heterojunction (Fig. 1). We employed tip sonication to exfoliate bulk TMDC, transforming it into a few-layered structure to increase the surface area. Initially, 300 mg of bulk TMDC powder purchased from Alfa Aesar was placed into 100 ml of isopropyl alcohol (IPA) and subjected to tip sonication for 4 h at 150 W power. The TMDC-containing beaker remained immersed in an ice and water mixture throughout the exfoliation process. Subsequently, the exfoliated TMDC solution underwent centrifugation at 2000 rpm for 1 h, yielding a supernatant enriched with few-layered TMDC. The resulting concentrations of the MoS_2 and WSe_2 dispersions were 0.06 and 0.075 mg/ml, respectively. The ZnO solution purchased from Sigma Aldrich was diluted to 0.06 mg/ml. The TMDC/ZnO heterojunction was confined to the dimensions of 4.2 mm × 1.85 mm using a shadow mask and annealed at 250 °C for 2 h in an Ar atmosphere to remove impurities. The finally prepared TMDC/ZnO heterojunction sample is shown in Fig. 1c.

Figure 2a, c demonstrate the TMDC nanosheets exfoliated through ultrasonic treatment with sizes predominantly ranging from 100 to 300 nm. These nanosheets are uniformly dispersed on a SiO_2 wafer, forming a compact and conductive network. The interstitial spaces between the TMDC nanosheets facilitate the penetration of NO_2 gas molecules, thereby leading to an increased number of adsorption sites for NO_2 gas. Figure 2b, d demonstrate randomly distributed ZnO nanoparticles (30–80 nm) on the TMDC nanosheets (indicated by red arrows). The SEM images of undiluted ZnO nanoparticles are featured

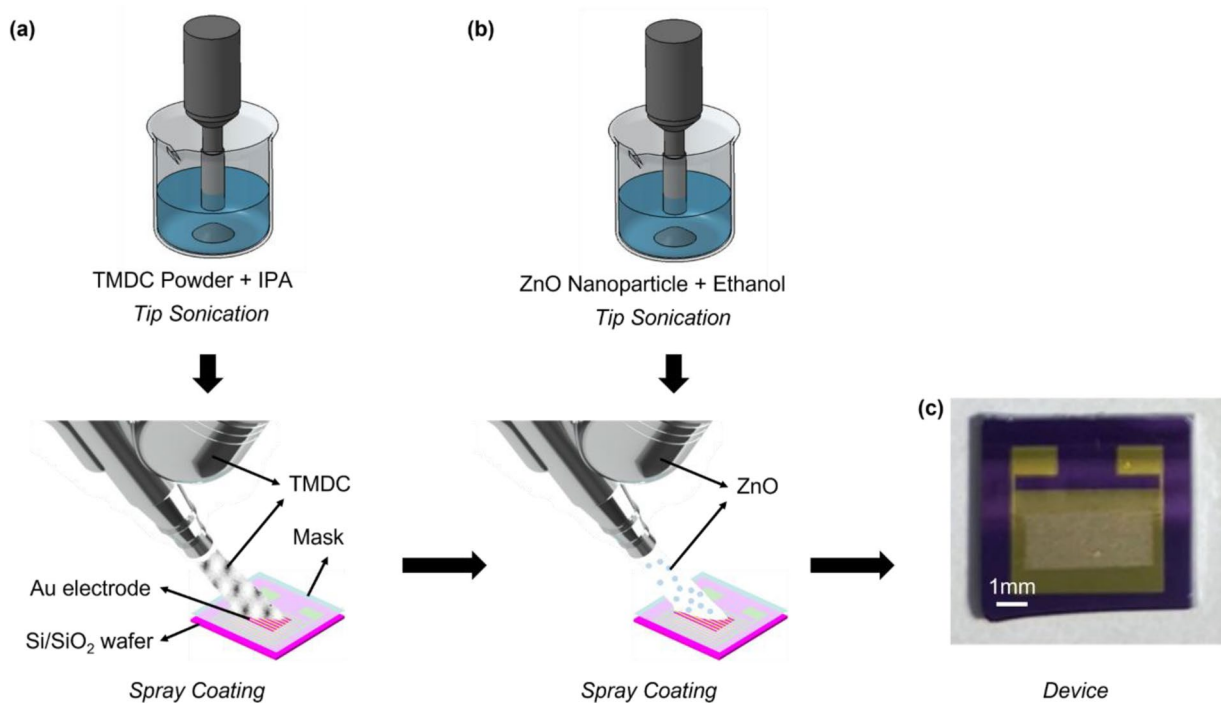

Fig. 1 Schematic of TMDC/ZnO-based NO_2 gas sensor fabrication process. (TMDC: transition metal dichalcogenides; IPA: Isopropylalcohol)

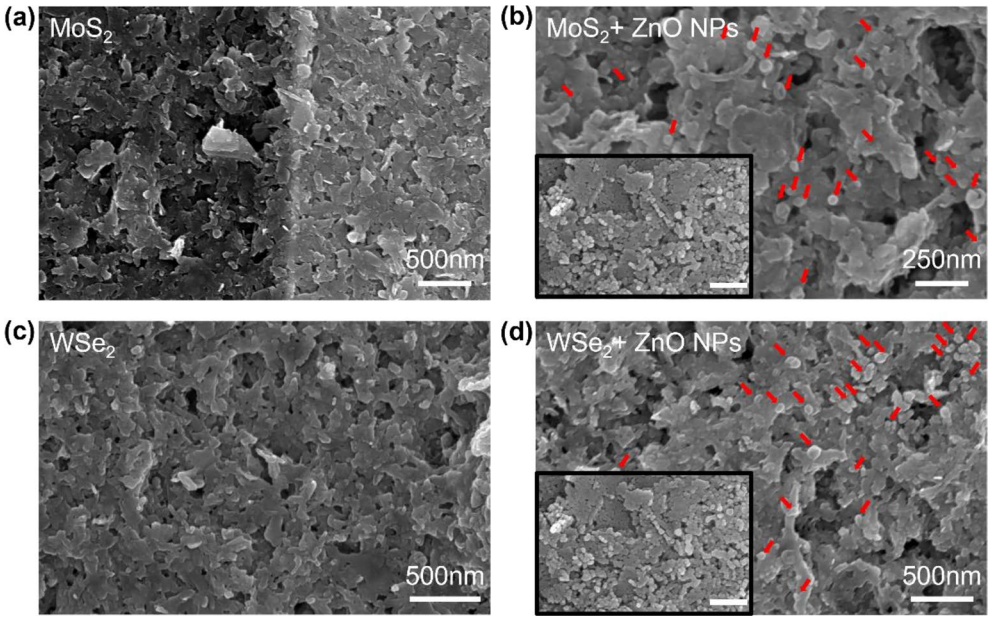

Fig. 2 Scanning electron microscopic images of **a** MoS_2-, **b** MoS_2/ZnO-, **c** WSe_2-, **d** WSe_2/ZnO-based gas sensors. The red arrow represents the ZnO nanoparticles (NP). The insets in **b** and **d** show SEM image of undiluted ZnO nanoparticles. The scale bars in the insets are 250 nm

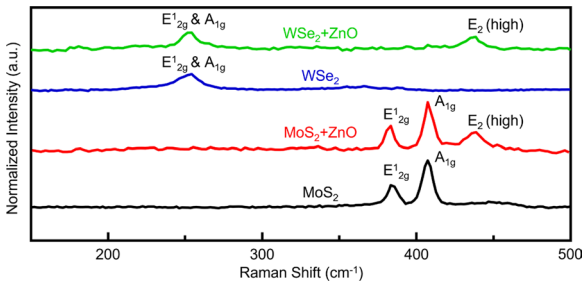

Fig. 3 Raman spectra of the transition metal dichalcogenides (TMDC)-based gas sensor (excited by 532 nm laser). Unlike TMDC, the TMDC/ZnO sensor exhibits the E_2 (high) characteristic peak of ZnO

in the inset of Fig. 2b, d. Aggregation of ZnO nanoparticles occurred due to its high concentration. On the other hand, we diluted and re-dispersed ZnO nanoparticles for sensor fabrication in order to minimize the aggregation of nanoparticles.

As shown in Fig. 3, the Raman spectrum of the TMDC-based gas sensor excited by a 532 nm laser exhibits prominent peaks of MoS_2 located at 407.41 and 383.4 cm^{-1}. These two peaks correspond to the out-of-plane (A_{1g}) and in-plane (E^1_{2g}) modes of MoS_2. The difference in the positions of these peaks is ~ 24.01 cm^{-1}, indicating the presence of a few-layered structure of the MoS_2 [51]. A single prominent Raman peak of WSe_2 appears at 254.3 cm^{-1}, which can be assigned to the overlapping of E^1_{2g} and A_{1g}, and indicates a few-layered structure of the WSe_2 [52]. Furthermore, the typical E_2 (high) peak of ZnO is observed at 438.2 cm^{-1} in MoS_2/ZnO and WSe_2/ZnO spectra [53], indicating the successful deposition of ZnO nanoparticles onto the TMDC nanosheets.

In this work, we used a custom-built gas chamber for conducting gas sensing experiments. This chamber is seamlessly integrated with both a gas mass flow controller and a temperature controller. Throughout the experimentation process, temperature was precisely maintained as the sample stage within the gas chamber was consistently maintained at 100 °C. To facilitate the experiments, the regulated flow of NO_2 gas and custom dry air was introduced through a mass flow controller. This ensured a steady total flow rate of 500 sccm. The I–V curves and resistance measurements of the gas sensor were accurately recorded using a Keithley 2634B sourcemeter. The TMDC/ZnO-based sensor exhibits a significantly higher resistance than the TMDC-based sensor, which can be attributed to the formation of heterojunctions (Fig. 4a, b). Furthermore, the addition of ZnO nanoparticles significantly reduces the signal drift of the TMDC-based sensor, whereas the response of the sensor remains unchanged (Fig. 4c). We studied the recovery rate of the sensors which can be defined as [54, 55]:

$$Recovery\ Rate = \frac{(I - I_{10min})}{(I - I_0)} \times 100\%$$

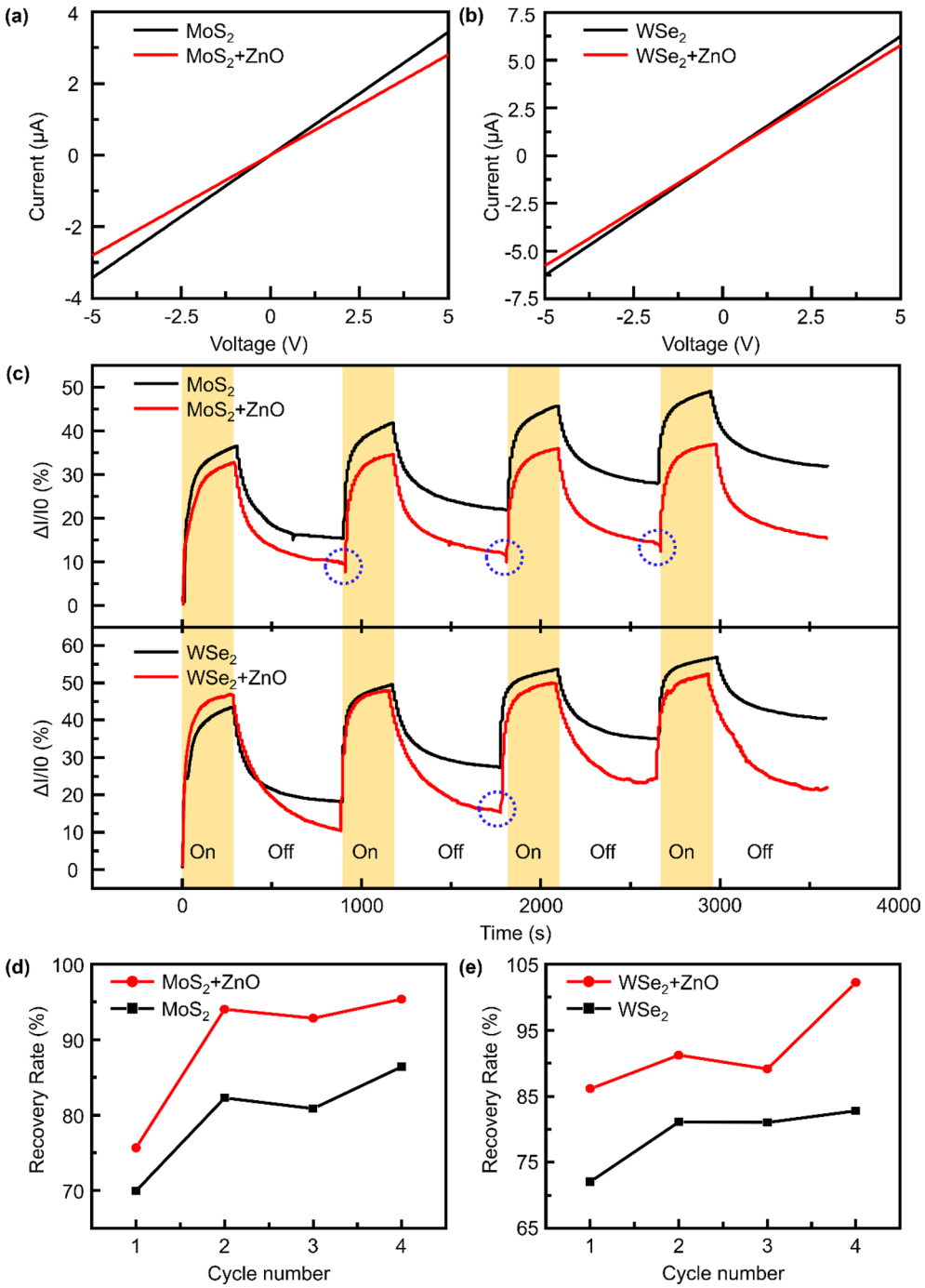

Fig. 4 I–V characteristics of **a** MoS_2^-, MoS_2/ZnO^-, **b** WSe_2^- and WSe_2/ZnO-based gas sensor in air environment at 100 °C. **c** Gas sensing response of transition metal dichalcogenides (TMDC)-based gas sensor to 10 ppm NO_2 gas at 100 °C. The part where the conductivity decreased at the early stage of NO_2 exposure is outlined by the blue dotted line. **d** Recovery rate per cycle of MoS_2^- and MoS_2/ZnO-based gas sensor. **e** Recovery rate per cycle of WSe_2^- and WSe_2/ZnO-based gas sensor

while I_0 is the initial current of the sensor, I is the current generated by the sensor exposed to NO_2 gas, and I_{10min} is the current of the sensor after shutting off the NO_2 gas for 10 min. Compared with MoS_2 and WSe_2, the recovery rates of MoS_2/ZnO and WSe_2/ZnO sensors improved by ~ 5.72–11.87% and ~ 8.10–19.44%, respectively (Fig. 4d, e). This is attributed to the variation in

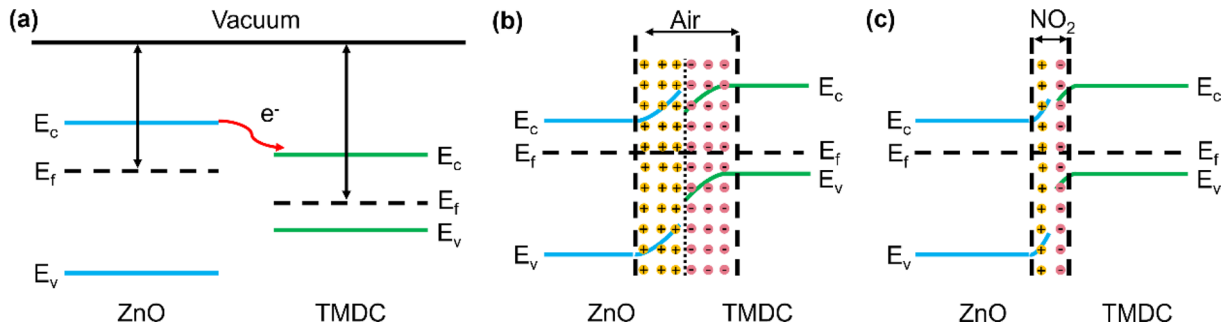

Fig. 5 Band diagrams of transition metal dichalcogenides (TMDC)/ZnO heterojunction **a** before equilibrium, **b** after equilibrium in air and **c** NO_2 gas atmosphere

the built-in field inside the heterojunction between the n-type ZnO and p-type TMDC.

The electrons of ZnO near the ZnO/TMDC interface tend to diffuse into TMDC, whereas the holes in TMDC tend to diffuse into ZnO before the Fermi levels of the p-type TMDC and n-type ZnO reach equilibrium (Fig. 5a). This leads to the formation of a depletion layer on the ZnO surface that gradually generates an internal electric field in the ZnO/TMDC interface region The internal electric field hinders further diffusion of carriers (Fig. 5b). When the sensor is exposed to NO_2 gas, the NO_2 molecules first capture electrons from ZnO with large adsorption energy and increase the width of the built-in electric field, resulting in a decrease in the sensor conductivity at the initial stage of NO_2 gas influx (the parts inside the blue dotted line in Fig. 4c). As the influx of NO_2 gas continues, NO_2 molecules start capturing electrons from the p-type TMDC surface with many active sites. The balance of the built-in electric field is broken, the holes accumulated at the ZnO side return to TMDC, and the width of the built-in electric field decreases (Fig. 5c). Furthermore, the desorption of NO_2 molecules on ZnO with large adsorption energy is slow and incomplete when air is introduced. This significantly improves the recovery rate of TMDC/ZnO-based gas sensors. Nonetheless, incompletely desorbed NO_2 molecules are still present on TMDC. The recovery rate could be further improved by employing external light sources [56, 57].

Conclusion

In this study, heterojunctions were fabricated via spray-coating a small amount of n-type ZnO nanoparticles onto the p-type TMDC nanosheets. SEM images and Raman spectra confirmed the successful deposition of small ZnO nanoparticles onto the large TMDC nanosheets. Furthermore, the fabricated heterojunction successfully improved the recovery rate of MoS_2/ZnO and WSe_2/ZnO sensors by ~ 5.72–11.87% and ~ 8.10–19.44%, respectively. This study is expected to contribute to the development of high-performance NO_2 gas sensors.

Abbreviations

NO_2	Nitrogen dioxide
TMDC	Transition metal dichalcogenides
CNT	Carbon nanotube
SiO_2	Silicon dioxide

Acknowledgements

Not applicable.

Author contributions

LW: contributed to synthesis, analysis, writing of the manuscript. JC: contributed to, Conceptualization, validation, Writing-review and editing.

Funding

This research was supported by the Basic Science Research Program of the National Research Foundation of Korea (NRF), funded by the Ministry of Science, ICT, and Future Planning (2022R1A2C4001577).

Availability of data and materials

The datasets used and/or analyzed during the current study are available from the corresponding author on request.

Declarations

Competing interests

The authors declare that they have no competing interests.

Received: 21 July 2023 Accepted: 28 August 2023
Published online: 11 September 2023

References

1. Bai M, Chen M, Li X, Wang Q (2022) One-step CVD growth of ZnO nanorod/SnO_2 film heterojunction for NO_2 gas sensor. Sens Actuators B 373:132738
2. Wang N, Tao W, Gong X, Zhao L, Wang T, Zhao L, Liu F, Liu X, Sun P, Lu G (2022) Highly sensitive and selective NO_2 gas sensor fabricated from Cu_2O-CuO microflowers. Sens Actuators B 362:131803
3. Xiong Y, Lu W, Ding D, Zhu L, Li X, Ling C, Xue Q (2017) Enhanced room temperature oxygen sensing properties of LaOCl-SnO_2 hollow spheres by UV light illumination. ACS Sens 2:679–686

4. Patil VL, Vanalakar SA, Shendage SS, Patil SP, Kamble AS, Tarwal NL, Sharma KK, Kim JH, Patil PS (2019) Fabrication of nanogranular TiO_2 thin films by SILAR technique: application for NO_2 gas sensor. Inorg Nano Metal Chem 49:191–197
5. Navale YH, Navale ST, Stadler FJ, Ramgir NS, Patil VB (2019) Enhanced NO_2 sensing aptness of ZnO nanowire/CuO nanoparticle heterostructure-based gas sensors. Ceram Int 45:1513–1522
6. Lee WS, Choi J (2019) Hybrid integration of carbon nanotubes and transition metal dichalcogenides on cellulose paper for highly sensitive and extremely deformable chemical sensors. ACS Appl Mater Interfaces 11:19363–19371
7. Ko KY, Song J-G, Kim Y, Choi T, Shin S, Lee CW, Lee K, Koo J, Lee H, Kim J, Lee T, Park J, Kim H (2016) Improvement of gas-sensing performance of large-area tungsten disulfide nanosheets by surface functionalization. ACS Nano 10:9287–9296
8. Lee WS, Choi, J (2019) Two-dimensional tungsten diselenides integrated on paper substrate for highly flexible and sensitive gas sensor. In: 2019 20th international conference solid-state sensors, actuators microsystems eurosensors XXXIII, TRANSDUCERS 2019 EUROSENSORS XXXIII, IEEE, Berlin, Germany, 23–27 June 2019
9. Sayago I, Santos H, Horrillo MC, Aleixandre M, Fernández MJ, Terrado E, Tacchini I, Aroz R, Maser WK, Benito AM, Martínez MT, Gutiérrez J, Muñoz E (2008) Carbon nanotube networks as gas sensors for NO_2 detection. Talanta 77:758–764
10. Kumar D, Chaturvedi P, Saho P, Jha P, Chouksey A, Lal M, Rawat JSBS, Tandon RP, Chaudhury PK (2017) Effect of single wall carbon nanotube networks on gas sensor response and detection limit. Sens Actuators B 240:1134–1140
11. Seekaew Y, Phokharatkul D, Wisitsoraat A, Wongchoosuk C (2017) Highly sensitive and selective room-temperature NO_2 gas sensor based on bilayer transferred chemical vapor deposited graphene. Appl Surf Sci 404:357–363
12. Pearce R, Iakimov T, Andersson M, Hultman L, Spetz AL, Yakimova R (2011) Epitaxially grown graphene based gas sensors for ultra sensitive NO_2 detection. Sens Actuators B 155:451–455
13. Alam MN, Kumar V, Lee D-J, Choi J (2023) Synergistically toughened silicone rubber nanocomposites using carbon nanotubes and molybdenum disulfide for stretchable strain sensors. Compos Part B Eng 259:110759
14. Wang L, Choi J (2022) Highly stretchable strain sensors with improved sensitivity enabled by a hybrid of carbon nanotube and graphene. Micro Nano Syst Lett 10:17
15. Lee SW, Lee W, Hong Y, Lee G, Yoon DS (2018) Recent advances in carbon material-based NO_2 gas sensors. Sens Actuators B 255:1788–1804
16. Hong HS, Phuong NH, Huong NT, Nam NH, Hue NT (2019) Highly sensitive and low detection limit of resistive NO_2 gas sensor based on a MoS_2/graphene two-dimensional heterostructures. Appl Surf Sci 492:449–454
17. Choi J, Kim J (2015) Defective carbon nanotube-silicon heterojunctions for photodetector and chemical sensor with improved responses. J Micromech Microeng 25:115004
18. Li Z, Li H, Wu Z, Wang M, Luo J, Torun H, Hu P, Yang C, Grundmann M, Liu X, Fu YQ (2019) Advances in designs and mechanisms of semiconducting metal oxide nanostructures for high-precision gas sensors operated at room temperature. Mater Horiz 6:470–506
19. Zhang Z, Haq M, Wen Z, Ye Z, Zhu L (2018) Ultrasensitive ppb-level NO_2 gas sensor based on WO_3 hollow nanosphers doped with Fe. Appl Surf Sci 434:891–897
20. Zhou P, Shen Y, Lu W, Zhao S, Li T, Zhong X, Cui B, Wei D, Zhang Y (2020) Highly selective NO_2 chemiresistive gas sensor based on hierarchical In_2O_3 microflowers grown on clinoptilolite substrates. J Alloys Compd 828:154395
21. Bhati VS, Ranwa S, Fanetti M, Valant M, Kumar M (2018) Efficient hydrogen sensor based on Ni-doped ZnO nanostructures by RF sputtering. Sens Actuators B 255:588–597
22. Wang J, Shen Y, Li X, Xia Y, Yang C (2019) Synergistic effects of UV activation and surface oxygen vacancies on the room-temperature NO_2 gas sensing performance of ZnO nanowires. Sens Actuators B 298:126858
23. Lu W-C, Kumar SS, Chen Y-C, Hsu C-M, Lin H-N (2019) Au/Cu_2O/ZnO ternary nanocomposite for low concentration NO_2 gas sensing at room temperature. Mater Lett 256:126657
24. Öztürk S, Kilinç N, Taşaltin N, Öztürk ZZ (2011) A comparative study on the NO_2 gas sensing properties of ZnO thin films, nanowires and nanorods. Thin Solid Films 520:932–938
25. Chang C-J, Lin C-Y, Chen J-K, Hsu M-H (2014) Ce-doped ZnO nanorods based low operation temperature NO_2 gas sensors. Ceram Int 40:10867–10875
26. Kaneti YV, Yue J, Jiang X, Yu A (2013) Controllable synthesis of ZnO nanoflakes with exposed ($10\bar{1}0$) for enhanced gas sensing performance. J Phys Chem C 117:13153–13162
27. Zhao S, Wang G, Liao J, Lv S, Zhu Z, Li Z (2018) Vertically aligned MoS_2/ZnO nanowires nanostructures with highly enhanced NO_2 sensing activities. Appl Surf Sci 456:808–816
28. Tamvakos A, Korir K, Tamvakos D, Calestani D, Cicero G, Pullini D (2016) NO_2 gas sensing mechanism of ZnO thin-film transducers: Physical experiment and theoretical correlation study. ACS Sens 1:406–412
29. Lee K, Baek D-H, Na H, Choi J, Kim J (2018) Simple fabrication method of silicon/tungsten oxide nanowires heterojunction for NO_2 gas sensors. Sens Actuators B 265:522–528
30. Lee E, Yoon YS, Kim D-J (2018) Two-dimensional transition metal dichalcogenides and metal oxide hybrids for gas sensing. ACS Sens 3:2045–2060
31. Agrawal AV, Kumar N, Kumar M (2021) Strategy and future prospects to develop room-temperature-recoverable NO_2 gas sensor based on two-dimensional molybdenum disulfide. Nano Micro Lett 13:38
32. Goswami P, Gupta G (2022) Recent progress of flexible NO_2 and NH_3 gas sensors based on transition metal dichalcogenides for room temperature sensing. Mater Today Chem 23:100726
33. Guo R, Han Y, Su C, Chen X, Zeng M, Hu N, Su Y, Zhou Z, Wei H, Yang Z (2019) Ultrasensitive room temperature NO_2 sensors based on liquid phase exfoliated WSe_2 nanosheets. Sens Actuators B 300:127013
34. Sharma I, Kumar KN, Choi J (2023) Highly sensitive chemiresistive detection of NH_3 by formation of WS_2 nanosheets and SnO_2 quantum dot heterostructures. Sens Actuators B 375:132899
35. Han Y, Huang D, Ma Y, He G, Hu J, Zhang J, Hu N, Su Y, Zhou Z, Zhang Y, Yang Z (2018) Design of hetero-nanostructures on MoS_2 nanosheets to boost NO_2 room-temperature sensing. ACS Appl Mater Interfaces 10:22640–22649
36. Kumar RR, Murugesan T, Dash A, Hsu C-H, Gupta S, Manikandan A, Anbalagan A, Lee C-H, Tai N-H, Chueh Y-L, Lin H-N (2021) Ultrasensitive and light-activated NO_2 gas sensor based on networked MoS_2/ZnO nanohybrid with adsorption/desorption kinetics study. Appl Surf Sci 536:147933
37. Choi J, Zhang H, Choi JH (2016) Modulating optoelectronic properties of two-dimensional transition metal dichalcogenide semiconductors by photoinduced charge transfer. ACS Nano 10:1671–1680
38. Choi J, Zhang H, Du H, Choi JH (2016) Understanding solvent effects on the properties of two-dimensional transition metal dichalcogenides. ACS Appl Mater Interfaces 8:8864–8869
39. Li H, Yin Z, He Q, Li H, Huang X, Lu G, Fam DWH, Tok AIY, Zhang Q, Zhang H (2012) Fabrication of single- and multilayer MoS_2 film-based field-effect transistors for sensing NO at room temperature. Small 8:63–67
40. Lee K, Gatensby R, McEvoy N, Hallam T, Duesberg GS (2013) High-performance sensors based on molybdenum disulfide thin films. Adv Mater 25:6699–6702
41. Li H, Wu J, Yin Z, Zhang H (2014) Preparation and applications of mechanically exfoliated single-layer and multilayer MoS_2 and WSe_2 nanosheets. Acc Chem Res 47:1067–1075
42. Zhang D, Wu J, Li P, Cao Y (2017) Room-temperature SO_2 gas-sensing properties based on a metal-doped MoS_2 nanoflower: an experimental and density functional theory investigation. J Mater Chem A 5:20666–20677
43. Cho S-Y, Kim SJ, Lee Y, Kim J-S, Jung W-B, Yoo H-W, Kim J, Jung H-T (2015) Highly enhanced gas adsorption properties in vertically aligned MoS_2 layers. ACS Nano 9:9314–9321
44. Late DJ, Huang Y-K, Liu B, Acharya J, Shirodkar SN, Luo J, Yan A, Charles D, Waghmare UV, Dravid VP, Rao CNR (2013) Sensing behavior of atomically thin-layered MoS_2 transistors. ACS Nano 7:4879–4891
45. Cho S-Y, Koh H-J, Yoo H-W, Kim J-S, Jung H-T (2017) Tunable volatile-organic-compound sensor by using Au nanoparticle incorporation on MoS_2. ACS Sens 2:183–189
46. Long H, Harley-Trochimczyk A, Pham T, Tang Z, Shi T, Zettl A, Carraro C, Worsley MA, Maboudian R (2016) High surface area MoS_2/graphene

hybrid aerogel for ultrasensitive NO_2 detection. Adv Funct Mater 26:5158–5165
47. Cui S, Wen Z, Huang X, Chang J, Chen J (2015) Stabilizing MoS_2 nanosheets through SnO_2 nanocrystal decoration for high-performance gas sensing in air. Small 11:2305–2313
48. Shim Y-S, Kwon KC, Suh JM, Choi KS, Song YG, Sohn W, Choi S, Hong K, Jeon J-M, Hong S-P, Kim S, Kim SY, Kang C-Y, Jang HW (2018) Synthesis of numerous edge sites in MoS_2 via SiO_2 nanorods platform for highly sensitive gas sensor. ACS Appl Mater Interfaces 10:31594–31602
49. Liu C, Chen X, Luo H, Li B, Shi J, Fan C, Yang J, Zeng M, Zhou Z, Hu N, Su Y, Yang Z (2021) Highly sensitive and recoverable room-temperature NO_2 gas detection realized by 2D/0D MoS_2/ZnS heterostructures with synergistic effects. Sens Actuators B 347:130608
50. Jaiswal J, Sanger A, Tiwari P, Chandra R (2020) MoS_2 hybrid heterostructure thin film decorated with CdTe quantum dots for room temperature NO_2 gas sensor. Sens Actuators B 305:127437
51. Castellanos-Gomez A, van der Zant HSJ, Steele GA (2014) Folded MoS_2 layers with reduced interlayer coupling. Nano Res 7:572–578
52. Sahin H, Tongay S, Horzum S, Fan W, Zhou J, Li J, Wu J, Peeters FM (2013) Anomalous Raman spectra and thickness-dependent electronic properties of WSe_2. Phys Rev B 87:165409
53. Liu C, Qiu Y, Wang F, Wang K, Liang Q, Chen Z (2017) Design of core–shell-structured ZnO/ZnS hybridized with graphite-like C_3N_4 for highly efficient photoelectrochemical water splitting. Adv Mater Interfaces 4:1700681
54. Feng Z, Xie Y, Chen J, Yu Y, Zheng S, Zhang R, Li Q, Chen X, Sun C, Zhang H, Pang W, Liu J, Zhang D (2017) Highly sensitive $MoTe_2$ chemical sensor with fast recovery rate through gate biasing. 2D Mater 4:025018
55. Yang Z, Jiang L, Wang J, Liu F, He J, Liu A, Lv S, You R, Yan X, Sun P, Wang C, Duan Y, Lu G (2021) Flexible resistive NO_2 gas sensor of three-dimensional crumpled MXene $Ti_3C_2T_x$/ZnO spheres for room temperature application. Sens Actuators B 326:128828
56. Kang Y, Pyo S, Jo E, Kim J (2019) Light-assisted recovery of reacted MoS_2 for reversible NO_2 sensing at room temperature. Nanotechnology 30:355504
57. Tabata H, Matsuyama H, Goto T, Kubo O, Katayama M (2021) Visible-light-activated response originating from carrier mobility modulation of NO_2 gas sensors based on MoS_2 monolayers. ACS Nano 15:2542–2553

Publisher's Note